IOPscience iopscience.iop.org

Home Search Collections Journals About Contact us My IOPscience

Impact source identification in finite isotropic plates using a time-reversal method: experimental study

This article has been downloaded from IOPscience. Please scroll down to see the full text article.

2012 Smart Mater. Struct. 21 105025

(http://iopscience.iop.org/0964-1726/21/10/105025)

View the table of contents for this issue, or go to the journal homepage for more

Download details:
IP Address: 152.14.115.121
The article was downloaded on 21/01/2013 at 15:13

Please note that terms and conditions apply.

IOP PUBLISHING SMART MATERIALS AND STRUCTURES
Smart Mater. Struct. **21** (2012) 105025 (10pp) doi:10.1088/0964-1726/21/10/105025

Impact source identification in finite isotropic plates using a time-reversal method: experimental study

Chunlin Chen[1,2], Yulong Li[1] and Fuh-Gwo Yuan[2]

[1] School of Aeronautics, Northwestern Polytechnical University, Xi'an, 710072, People's Republic of China
[2] Department of Mechanical and Aerospace Engineering, North Carolina State University, Raleigh, NC 27695, USA

E-mail: yuan@ncsu.edu

Received 1 January 2012, in final form 29 July 2012
Published 24 August 2012
Online at stacks.iop.org/SMS/21/105025

Abstract
An impact source identification technique for finite isotropic plates using a time-reversal method with associated signal processing algorithms is investigated experimentally. A series of low velocity impact experiments on an aluminum plate is performed to verify this impact identification method using merely four piezoelectric sensors. Validation of the experimental system for impact source identification using the time-reversal method is first examined. Critical issues concerning the spacing of calibrated points, and associated problems, have been studied in detail. The appropriate spacing of the transfer function is determined and both the impact location and impact loading history are well estimated. The factors which affect the accuracy of impact location detection and force reconstruction are analyzed. The results of the impact identification experiments are repeatable and stable. The time-reversal method is suited to identifying impact events in plate-like structures.

(Some figures may appear in colour only in the online journal)

1. Introduction

One of the main objectives of impact source identification is to monitor impact events on structures and to predict their structural health. Impact location detection and impact force reconstruction are the two main objectives in impact source identification. Usually, the impact location is estimated prior to reconstructing the impact loading time-history. The most popular method for impact location detection is based on the time difference of the arrival of sensor signals received by a spatially distributed sensor array [1]. However, it is rather difficult to obtain the time-of-flight and wave velocity information accurately in practice. Park and Chang [2] estimated the impact location by mapping the power distribution over the entire structure using uniformly distributed sensors, thus requiring many sensors. Hu *et al* [3] determined the impact location by comparing numerical strains and experimental results among calibration points once the impact force had been approximated. The computation may be very complex for large structures. Neural networks [4] can be used to trace impact location because of their versatility, but a large amount of training data may be required. The time-reversal method [5, 6] has been recently utilized to locate acoustic emission sources and impact locations.

The impact force can be reconstructed indirectly by the sensor signals and the characteristic information of the structures, such as Green's function or the transfer function, which is the physical relationship between the impact force and its response. Based on these functions, a deconvolution technique is commonly used to solve this inverse problem in the time or frequency domain [7]. To handle the ill-conditioned nature of the inverse problem, regularization techniques have been developed in deconvolution computation [8, 9]. Seydel and Chang [10, 11] developed a model-based technique to predict both the

 © 2012 IOP Publishing Ltd Printed in the UK & the USA

location and force history of an impact on a stiffened panel. Impact force could be also computed by neural networks [12] without the need for transfer functions. However, the training process may be too complex to be practical because the training data should be generated in any type of loading history at all locations. Outstanding issues for impact source identification, such as the number of sensors, the mechanical properties of structures and the complexity of algorithms remain to be resolved.

An impact source identification technique using the time-reversal (T-R) method was developed in a theoretical study to monitor impact events in plate structures by the present authors [13]. Based on transfer functions, both the impact location and impact loading time-history are recovered by the T-R procedure and associated signal processing algorithms. The time duration of the T-R process, number and spatial distribution of sensors, reconstruction of force with various shapes and frequency were discussed in the theoretical study. When this identification system is implemented in practice, several issues must be investigated. One of the key challenges is how dense the plate needs to be calibrated to obtain transfer functions. For example, it is impractical to calibrate the transfer function with 10 mm spacing on a plate with in-plane dimensions of 700 mm $\times$ 700 mm. How is suitable spacing of the transfer functions for a given plate structure determined? The questions pertaining to the spacing of transfer functions, such as the accuracy of impact location detection under various spacings and the approximation of transfer functions for force reconstruction need to be studied. The second problem is the validation of this impact identification method for its application. How is the system validated before impact monitoring? The last question relates to the repeatability and stability of this system for impact detection on plate structures. In this experimental study, these issues for the application of impact identification techniques are discussed in detail.

2. T-R method for impact source identification

This technique for impact source identification based on the T-R concept is examined. In an ideal T-R model, the waves generated by the excited source are recorded as a time series of signals from a number of sensors, and then they are back-propagated (or time reversed) back into the medium. The reversed signals then focus back to their original source due to constructive interference, elucidating the impact location, extent, and impact source pattern (loading time-history).

To identify the impact source on plate-like structures by the T-R method, the transfer functions are first attained in a calibration procedure. After the plate is impacted, the impact response and transfer functions are computed in the T-R process. The information concerning the impact location and impact loading time-history is retrieved from the reconstructed signal at each calibration location. Viable methods to determine the impact location and to reconstruct the impact loading time-history after T-R processing will be discussed as follows. It is noted that no knowledge of the material properties or boundary conditions is required in the experiments.

The transfer function (Green's) which represents the relationship between the calibrated impact force and the strain response at a sensor location is calibrated in frequency domain by

$$G_i(\boldsymbol{\xi}, \omega) = \frac{S_i(\omega)}{F(\boldsymbol{\xi}, \omega)} \tag{1}$$

where $F(\boldsymbol{\xi}, \omega)$ is the calibration force at the location $\boldsymbol{\xi}$ and $S_i(\omega)$ is the summation of the in-plane strain response $(\varepsilon_x + \varepsilon_y)$ proportional to the output voltage measured by the ith piezoelectric sensor. The plate is calibrated by discrete calibration points (locations), evenly spaced within the enclosed sensor area.

Transfer functions between any two arbitrary points in the plate are reciprocal based on its spatial reciprocity. Mathematically the T-R procedure can be realized through transfer functions derived from equation (1), and the T-R procedure in the frequency domain can be expressed by

$$f_i(\boldsymbol{\xi}, \omega) = G_i^*(\boldsymbol{\xi}, \omega) s_i(\omega) = G_i(\boldsymbol{\xi}, \omega) s_i^*(\omega) \tag{2}$$

where $f_i(\boldsymbol{\xi}, \omega)$ is the reconstructed signal contributed by the measured strain $s_i(\omega)$ and the superscript (*) denotes the complex conjugate of the variable. The reconstructed signals at any point in the structure from all the sensors can be expressed in the time domain as

$$F(\boldsymbol{\xi}, T - t) = \sum_{i=1}^{n} f_i(\boldsymbol{\xi}, T - t) \tag{3}$$

where n is the number of sensors and T is the time duration of the T-R process. The proper choice of T and n has been discussed in [13].

2.1. Impact location detection

The T-R method is a temporal and spatial focusing technique; the maximum peak amplitude of the reconstructed signals will refocus at the impact location and at the corresponding time of the impact. The impact source can be identified by selecting the maximum peak amplitude of the reconstructed signals at each point in the plate during the entire time period. Since it is not practical to obtain the transfer function at every point in the plate, the critical issue is to select the appropriate spacing. An adaptive two-step search algorithm has been developed to trace the impact location. The plate is divided into small square areas by evenly spaced calibration points. An initial detection will be performed to roughly estimate the impact location by selecting the maximum peak amplitude of the reconstructed signals among the calibration locations, $\mathbf{x}_{jk} \equiv (x_j, y_k)$. Then the impact location is further searched in the impact area. The peak amplitude of the reconstructed signals $P(\mathbf{x}_{jk})$ is defined as

$$P(\mathbf{x}_{jk}) = \mathrm{Max}_{\text{at all times}}[F(\mathbf{x}_{jk}, T - t)] \tag{4}$$

The first approximate impact location, denoted by $\hat{\mathbf{x}}$, is determined by

$$Q(\hat{\mathbf{x}}) = \mathrm{Max}[P(\mathbf{x}_{jk})]. \tag{5}$$

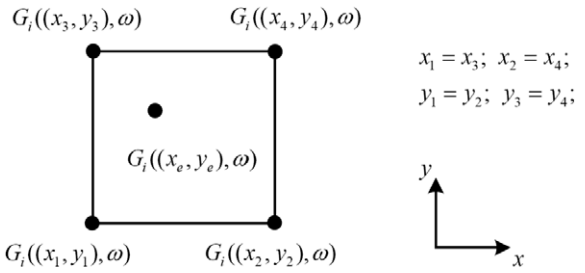

Figure 1. Approximated transfer function at the estimated impact location.

A finer search for the impact location is then conducted in the most probable impact area. Among the four areas sharing the approximate impact location, the impact area is chosen by the maximum peak amplitude at the calibration location (or approximate impact location) and three other relatively high peak amplitudes constituting the square area. The impact location is estimated in terms of the centroid of the peak amplitude of the reconstructed signals at four calibration locations. The centroid, $\hat{\hat{\mathbf{x}}}(x_e, y_e)$, is considered to be the finer impact location determined by

$$x_e = \frac{\sum_{j=1}^{4} x_j P(x_j, y_k)}{\sum_{j=1}^{4} P(x_j, y_k)}, \qquad y_e = \frac{\sum_{j=1}^{4} y_j P(x_j, y_k)}{\sum_{j=1}^{4} P(x_j, y_k)} \tag{6}$$

where P is the peak amplitude of the reconstructed signal at calibration locations which enclose the impact source.

2.2. Impact loading time-history reconstruction

The computation of the T-R method used in this work is a simple operation, and only the transfer function and strain response are used in the T-R process; thus only partial information concerning the force, such as the shape of the impact loading time-history, can be reconstructed. Based on transfer functions, the shape of the loading history and the impact location are obtained in the impact location estimation simultaneously.

In general the estimated impact location is not at the calibration locations exactly; the transfer functions need to be approximated. The transfer functions at the estimated location can be linearly interpolated [2] from transfer functions at four neighboring calibration locations given below and shown in figure 1.

$$G_i(\hat{\hat{\mathbf{x}}}, \omega) = \sum_{j=1}^{4} \eta_j G_i(\mathbf{x}_{jk}, \omega) \tag{7}$$

where $\eta_1 = (1-\alpha)(1-\beta)$, $\eta_2 = \alpha(1-\beta)$, $\eta_3 = (1-\alpha)\beta$, $\eta_4 = \alpha\beta$, $\alpha = (x - x_1)/(x_2 - x_1)$, $\beta = (y - y_3)/(y_3 - y_2)$.

Once the impact location and the shape of the impact force are obtained by the T-R method, the magnitude of the force can then be calculated by comparing the response signals measured by the sensors with the response signals predicted by the shape of the force and the transfer functions. The predicted response signals are computed by

$$S_i(\omega) = F(\hat{\hat{\mathbf{x}}}, \omega) G_i(\hat{\hat{\mathbf{x}}}, \omega). \tag{8}$$

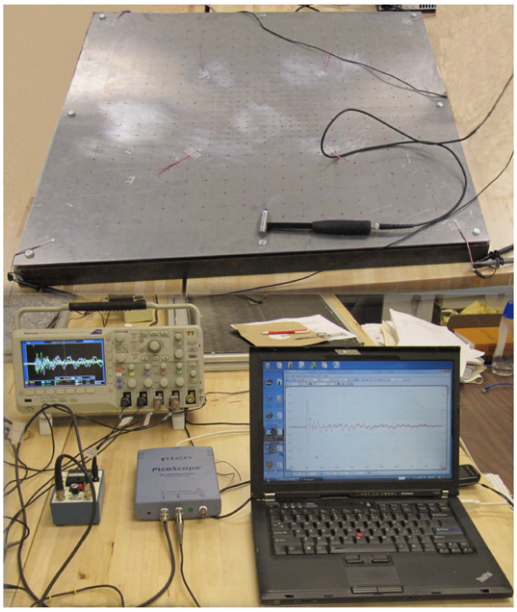

Figure 2. Experimental setup for impact source identification.

This computation is a forward process. The first estimated scaling factor $\hat{k}$ is calculated as

$$\hat{k} = \frac{1}{n} \sum_{i=1}^{n} \left[\frac{\sum_{t=0}^{T} |s_i(t)|}{\sum_{t=0}^{T} |S_i(t)|} \right] \tag{9}$$

where $s_i(t)$ is the response signal measured by the sensors and $S_i(t)$ is the predicted response signal in the time domain. Then a finer magnitude search algorithm based on a least-squares method is proposed to more accurately determine the magnitude of the force. It is written as

$$E(k) = \frac{1}{n} \sum_{i=1}^{n} \left[\sum_{t=0}^{T} |s_i(t)|^2 - k^2 \sum_{t=0}^{T} |S_i(t)|^2 \right]. \tag{10}$$

The minimum amplitude of $E(k)$ is calculated as $E(\hat{\hat{k}})$ in the range $[0.5\hat{k}, 1.5\hat{k}]$.

As the impact location detection was based on the selection of the maximum peak magnitude of the reconstructed signals, the approximated transfer functions cannot be used for impact location detection. Considering the impact force normal to the plate and the main impact energy is in the main packet wave in practice, only the main packet wave is selected for reconstructing the shape of the impact force in experiments.

3. Experiments

3.1. Experimental setup

The impact source identification by the T-R method was verified experimentally on a flat aluminum plate. Figure 2 shows the experimental setup. A plate with dimensions 914.4 mm × 914.4 mm × 3.1 mm was fixed on a steel frame by eight screws around the edges of the plate. Four

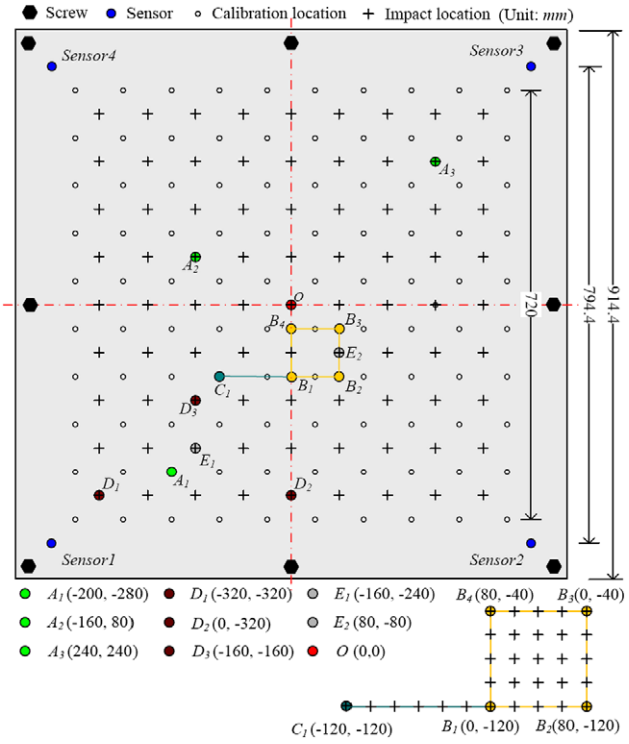

Figure 3. Sensor, impact, and calibration locations with 80 mm spacing and other locations to be discussed in the aluminum plate.

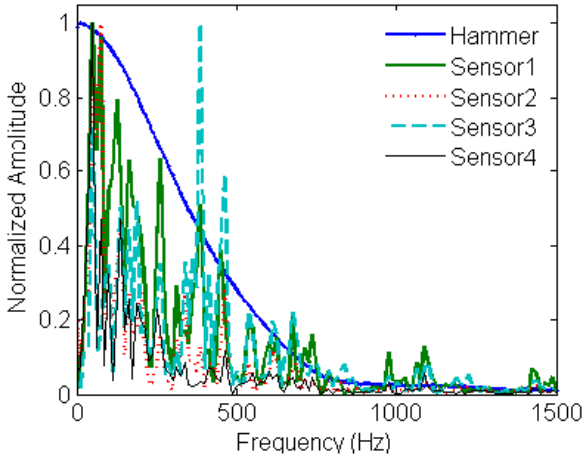

Figure 4. Frequency domain analysis of voltage signals in one impact event at the A_1 $(-200, -280)$ location.

piezoelectric sensors (diameter: 7 mm; thickness: 0.3 mm) were mounted near the corner of the plate, 60 mm from each side of the plate. The impact responses from the sensors were recorded by a Digital Phosphor oscilloscope (model: DPO 2024; manufacturer: Tektronix, Inc.). The impact force from a hand-held instrumented hammer (model: 086C02; manufacturer: PCB Piezotronics, Inc.) was recorded by a data acquisition system (model: PicoScope 3206; manufacturer: Pico Technology). The sampling rate was set to 50 kHz. The time duration of the measurement was 100 ms. The in-plane strain response ($\varepsilon_x + \varepsilon_y$) and the impact force are proportional to the output voltage of the piezoelectric sensor and the instrumented hammer, respectively. The measured voltage signals were processed directly to demonstrate the T-R method for impact source identification. It is noted that all the impact forces are generated by the impact hammer with a medium impact cap. The forces strike normal to the plate surface without inducing impact damage on the plate after impact. Figure 3 shows the sensor locations, calibration locations, and impact locations on the plate for the spacing of the calibration location being 80 mm marked by open circles, which will be discussed later.

3.2. Validation of experimental system

The previous theoretical study [13] by the authors has demonstrated that the T-R method is a powerful technique for impact source identification. However, subtle differences between numerical simulation and experiments that may affect the self-focusing capability of the T-R method should be resolved prior to the impact monitoring. The issues are included as follows. (1) The impact experiments by the impact hammer contact a small plate area, not a point as performed in simulations. (2) The output of the piezoelectric sensors is related to the integral of the sum of the in-plane strains on the sensor surface, not the strain values in the simulation. (3) The uniformity of the sensor quality, such as the adhesive condition, the electromechanical parameters and the electric connection condition. (4) The boundary conditions of the plate were more complex than that of the simulation. (5) Damping of the structures existed in experiments, which had been neglected in simulation; and (6) The impact was carried out using a hand-held electronic hammer.

To ensure the impact identification experiments are reliable, some validation work of the experimental system had been conducted before impact identification. The response of the sensors, the linearity of the transfer functions, and the self-focusing capability of the T-R method were considered. In low velocity impact experiments, the frequency bands of the strain response correspond to that of the impact force. Figure 4 shows the frequency domain analysis of voltage signals from PZT sensors for the impact hammer impacting at location A_1. The main energy of the sensors' signals concentrated on low frequency bands less than 1 kHz, which was consistent with that of the hammer signals. The results at other calibration locations were similar to that of A_1. The conditions of the PZT sensors were good for measurement. The T-R method for impact force identification on plate-like structures was based on the transfer functions. The results of the T-R procedure were related to the linearity of the transfer functions. Figure 5 shows the empirical transfer functions between the impact force at location A_2 and Sensor2 under five impact events. A good repeatability of the transfer function is obviously seen in this figure. The results of the transfer functions between other calibration locations and sensors were similar. In impact source identification, both the impact location detection and force reconstruction depended on the self-focusing capability of the T-R method. Figure 6 shows the reconstructed impact signals at location A_3. The signals focused at the impact time and the shape of

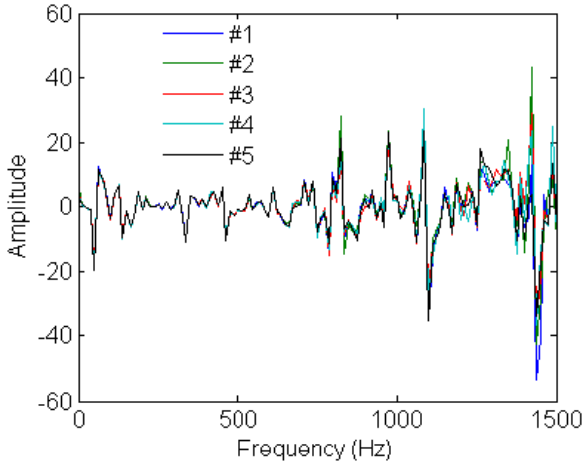

Figure 5. Transfer functions between impact force at location A_2 and Sensor2 five times.

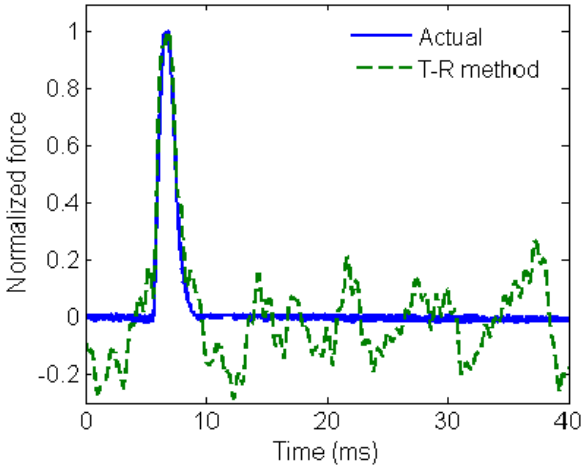

Figure 6. Reconstruction of impact force shape at location A_3.

the main wave packet of the impact force was reconstructed successfully. After experimental validation, the next step is the calibration of transfer functions.

3.3. Transfer function calibration and impact test

In previous work [14], the resolution of impact identification was dependent on the density of calibration points. More information concerning impact source identification can be obtained when the calibration locations are denser. However, the number of calibration locations and the time spent in computation for force identification will increase dramatically with the increase of the calibration density. In impact experiments, it is also impractical to obtain the transfer functions at many locations of the plate. Thus, the spacing of the calibration location is a critical factor for impact identification.

In simulation [14], the permissible spacing of the calibration location on the aluminum plate with 1 mm thickness was 40 mm. The permissible spacing of the calibration location increased increasing plate thickness. To find the appropriate spacing of the calibration locations on this flat aluminum plate, a square area (240 mm $\times$ 240 mm) around the center of the plate was calibrated with the spacing 40 mm in trial experiments. This square area was divided into 6 $\times$ 6 small square areas by the calibration locations. In each small square area, the impact hammer struck at the center of the area. The results showed that all the impact locations could be detected at the actual impact area successfully when the spacing of the calibration location was 40 mm and 80 mm respectively. Thus, the spacing of the calibration on the entire plate began from 80 mm. In the trial experiment, the time duration of the T-R process was 40 ms and the truncation frequency was 1.5 kHz. The choices of the time duration of the T-R method and the truncation frequency have been discussed in the simulation work [13]. The accuracy of the transfer functions increases with increasing calibration time at each calibration location. However, the computational effort and impacts also increase rapidly with increasing calibration times. On the entire plate, each calibration location was impacted twice and the transfer functions were obtained from the averaged one. The results of impact source identification with various calibration location spacings will be discussed in detail in the next section. Note in the following, the unit mm for the coordinates will be used and will be dropped hereafter unless otherwise stated.

4. Results and discussion

4.1. Results of the impact location detection

The spacing of the transfer function calibration locations was selected starting from 80 mm. To determine the appropriate spacing of the calibration location and the relation between the impact location detection and the density of the transfer function calibrations, uniformly distributed impact locations were detected under various calibration spacings, 80, 120, and 160 mm. When the spacing was 80 mm, the entire plate was divided into 9 $\times$ 9 small square areas. Eighty-one impact events were located at the center of each square area once. In the initial search step, among the 81 impact events, almost all the maximum peak values of the reconstructed signals appeared at the one of the four actual calibration locations which was nearest to the actual impact location, except two impact events at (240, 80) and (80, 240) were searched at (200, 200). In the finer search step, most of the impact events, 75 out of 81, were detected at the actual impact area, and the remaining six events were detected at the neighboring square areas.

Figure 7 shows the deviation of impact location detection. The average error of the impact location detection was 3.5 mm if detected at the actual impact area. The average error of location detection was 76.3 mm if detected at the neighboring impact area and the average error of location detection for all impact events was 8.9 mm. When the remaining events were detected in the neighboring impact areas, the sum of the peak value of the four reconstructed signals in the detected impact area and the actual impact area were very close to each

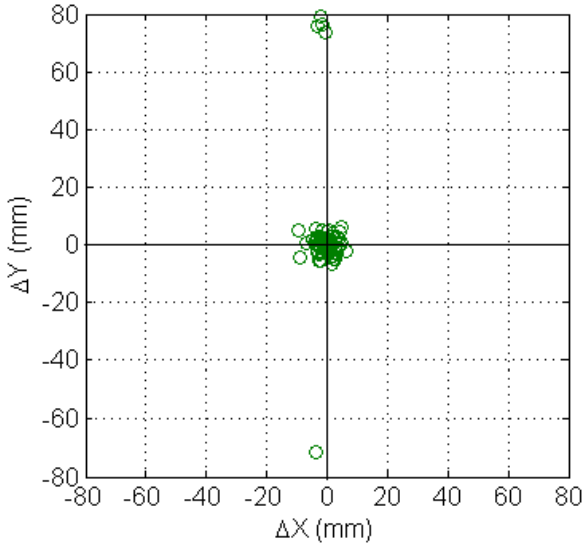

Figure 7. Discrepancy in impact location detection when the spacing is 80 mm.

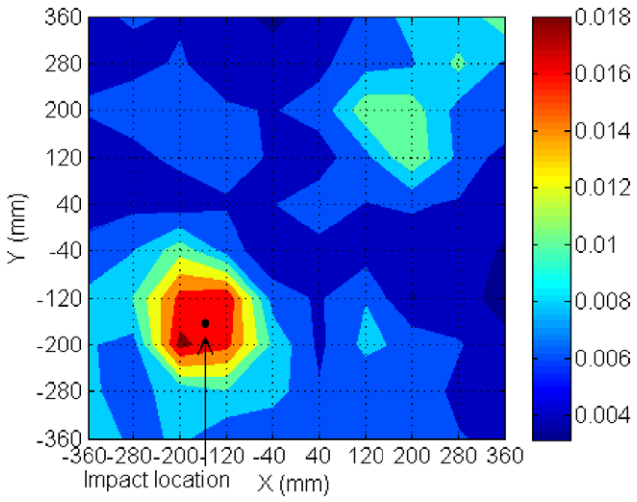

Figure 8. Contour plot of the peak value of the reconstructed signals for impact loaded at (−160, −160) when the spacing is 80 mm.

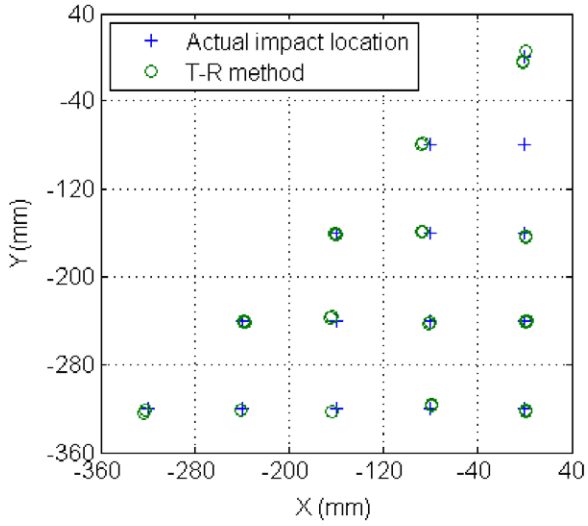

Figure 9. Results of impact location detection in the one-eighth region of the plate three times under 80 mm spacing.

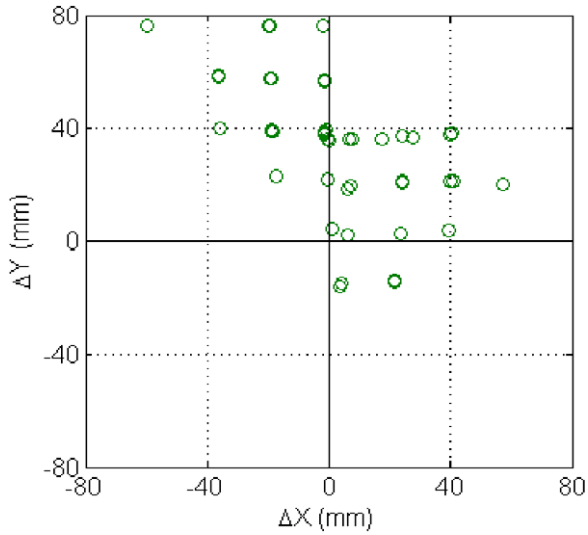

Figure 10. Discrepancy in impact location detection in area $B_1B_2B_3B_4$ when the spacing is 80 mm.

other. Figure 8 shows a contour plot of the peak value of the reconstructed signals for an impact loaded at (−160, −160); the maximum peak value of the reconstructed signal was at (200, −200) and the detected impact location was (−160.6, −160.4). It is obvious that the area with the higher peak value of the reconstructed signal (red area) covered the impact location. For other impact events, the results were similar.

The deviation in experiments that may be caused by the condition of the sensors, environment noise, manual actions and so on cannot be avoided completely though the experimental system had been validated. To investigate the reliability of the impact identification system, impacts were loaded at the center of 15 small impact areas three times. Figure 9 shows the results of the impact location detection on the one-eighth portion of the plate. Most impact events were detected at the actual impact area except one (0, −80), which was detected at the neighboring impact areas. It is noted that the repeatability of impact location detection at each impact area is very good.

In the above impact location detection, all the impacts were loaded at the center of each small square area whose vertices are four calibration points. However, the impact event may strike at any point of the plate including the calibration points. Twenty-five points in one square area $B_1\,B_2\,B_3\,B_4$ shown in figure 3 with spacing 20 mm were impacted twice to investigate the capability of the T-R method for impact location detection. These points are distributed in two impact areas. Figure 10 shows the discrepancy of the impact location detection. All the impacts were detected at the correct or neighboring impact areas. The mean error of impact location detection is 42.1 mm. The resolutions of impact location detection were less accurate in comparison with the cases when the impacts were at the center of each small square area. As the output of the PZT sensor represented the strain of the

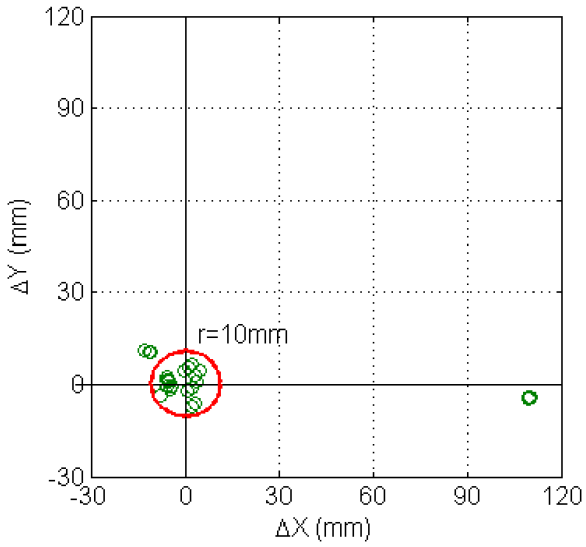

Figure 11. Discrepancy in impact location detection when the spacing is 120 mm.

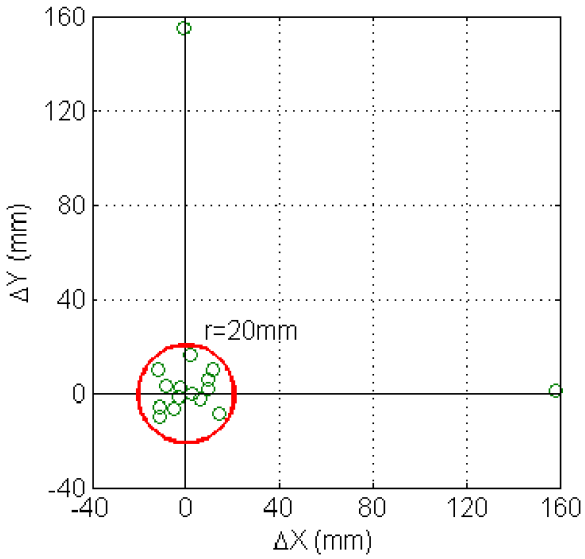

Figure 12. Discrepancy in impact location detection when the spacing is 160 mm.

area it covered, the difference in these transfer functions at two nearby calibration points may be minor, which would lead to the reconstructed signals at the calibration points quite near the actual impact locations being similar and more impacts being detected at the center of the actual or neighboring impact areas. In impact source location detection by the T-R method on plate-like structures, the impact points may not be covered by the detected impact area because of the slight difference of the reconstructed signals at calibration points which were near to the actual impact point. Thus, more information concerning the reconstructed signals in the T-R process will be used to trace the impact location in the future.

For the spacing of the transfer function calibration location being 80 mm, all the impact locations can be identified successfully. The results show the good reliability of the T-R method for impact location detection. In previous simulation work [14], the error of the impact location detection increases with increasing transfer function spacing. Figure 11 shows the results of the impact location determination when the spacing is 120 mm, where the radius of the red circle is 10 mm. Similar to that of 80 mm, most of the impact events were detected at the actual impact area except a few that were detected at the neighboring impact areas. The average error of the impact location detection was 6.7 mm if they were detected at the correct impact area. The average error of location detection was 110.1 mm if detected at the neighboring impact area and the average error of location detection for all impact events was 18.2 mm. Figure 12 shows the results of the impact location determination when the spacing is 160 mm, where the radius of the red circle is 20 mm. Only two locations (40, 200) and (200, 40) were detected at the neighboring impact areas. The average error in impact location detection was 10.4 mm if the correct impact areas had been detected. The average error of location detection was 156.7 mm if detected at the neighboring impact area and the average error of location detection for all impact events was 28.7 mm. Table 1 shows the average error of impact location detection and the success rate of impact area detection under various calibration spacing. As expected, the impact location detection error and the standard deviation increase with decreasing transfer function density. The successful rate of correct impact area detection increases with the increase of the density of the calibrated transfer functions from 160 to 80 mm.

Table 1. Impact location detection under various calibration spacings.

Calibration spacing (mm)	80	120	160
Error in impact location (mm)	8.9	20.2	28.7
Standard deviation (mm)	19.2	35.0	48.6
Success rate of impact area	25/27	8/9	7/8

4.2. Force reconstruction

In the simulation work [14], the resolution of the impact loading time-history reconstruction depends on the accuracy of the impact location detection. In this section, the impact forces at various locations were identified under the spacing 80 mm first. The repeatability of the T-R method for impact force reconstruction was validated by impacting the location E_1 three times. To investigate the effect of approximated transfer functions on force reconstruction, the impact force at location E_2 was identified by various transfer functions. Finally, the error of impact location detection on force reconstruction is discussed followed by some suggestions about the selection of the transfer function spacing.

Upon the impact location detected at $\hat{\mathbf{x}}$, the transfer functions $G_i(\hat{\mathbf{x}}, \omega)$ between the detected impact location and the sensors can be approximated by equation (7). Then the shape of the force can be reconstructed by the approximated transfer functions in the T-R process. In the final step, the scaling factor of the force was determined by the method

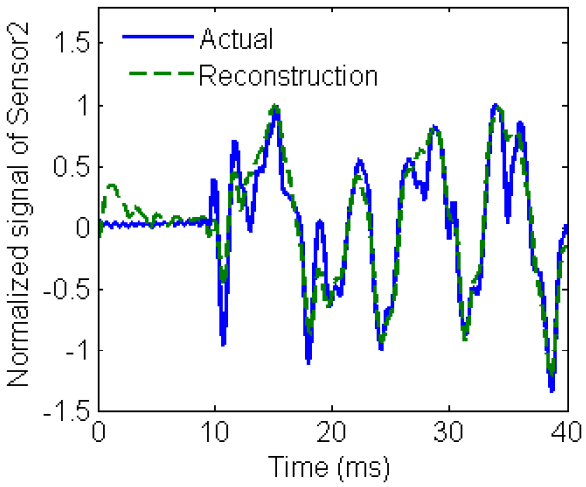

Figure 13. Shape of strain response measured by Sensor2 and reconstructed by the T-R method.

developed in the previous section. Figure 13 shows the strain measured by *Sensor2* and the one reconstructed by transfer functions and the shape of the impact loading time-history, where the actual impact location was D_2 and the estimated impact location was (0.8, −322.7). Due to the good reconstruction of the strain response, the magnitude of the impact force can identified. The reconstructed force at location D_1, D_2, D_3, and O are shown in figure 14. The main information about the forces was identified successfully. Similar results are obtained from the other remaining locations. In impact loading time-history reconstruction, there were some deviations in both the shape and scaling factor determination between the actual and reconstructed impact loading time-history. The deviation may be attributed to the error in impact location detection, transfer function approximation, and the system deviations of the T-R method. The errors in impact location detection at points D_1, D_2, D_3, and O were close to each other and less then 6 mm. Thus, the error of the force reconstruction mainly depends on the relative position of the impact location in the plate.

Figure 15 shows the reconstruction of the impact loading time-history by impacting at point E_1 three times. The starting times of these impacts' loading time-histories are intentionally shifted to make them more clear in one figure. The resolution of impact location detection at this point is shown in figure 9. Impact forces with various magnitudes

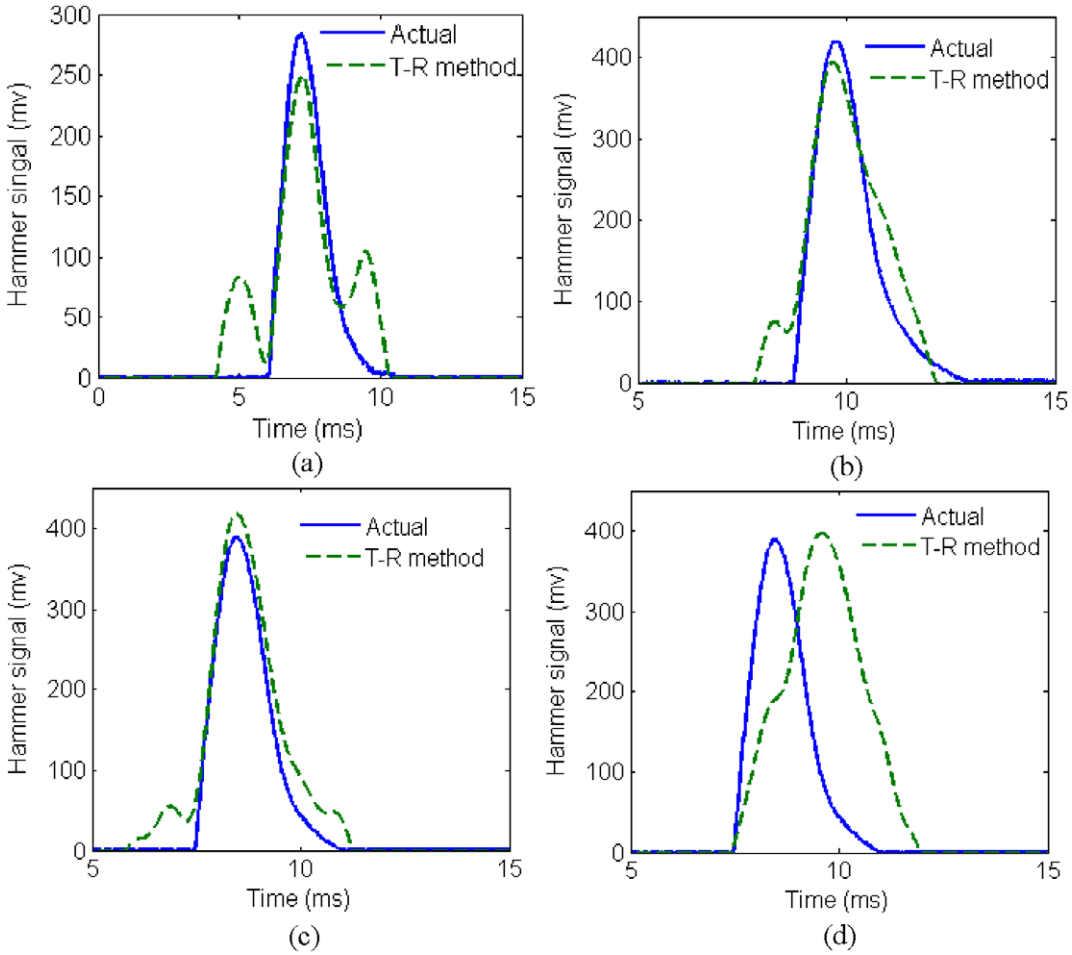

Figure 14. Impact force time-history reconstructions at various impact locations. (a) D_1 (−320, −320), (b) D_2 (0, −320), (c) D_3 (−160, −160), (d) O (0, 0).

Table 2. Peak force identification under with various distances from the actual impact location.

Distance (mm)	Actual	0	20	40	60	80	100	120
Peak voltage (mV)	603.4	528.3	543.1	575.6	560.8	512.4	415.7	337.4
Error (%)	0	−12.4	−10.0	−4.6	−7.1	−15.1	−31.1	−44.1

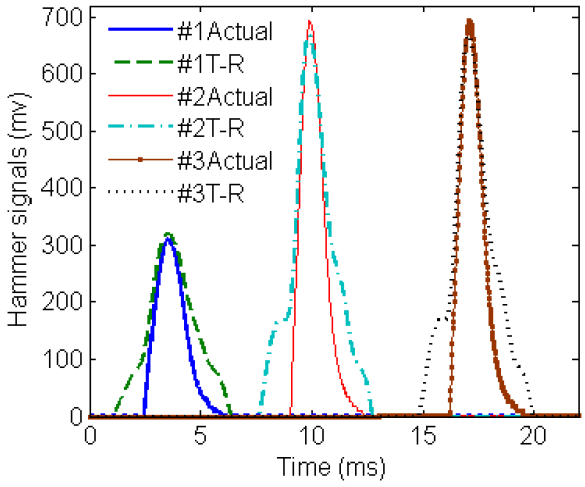

Figure 15. Comparison of actual and reconstructed impact force time-history by impacting at E_1 (−160, −240) three times.

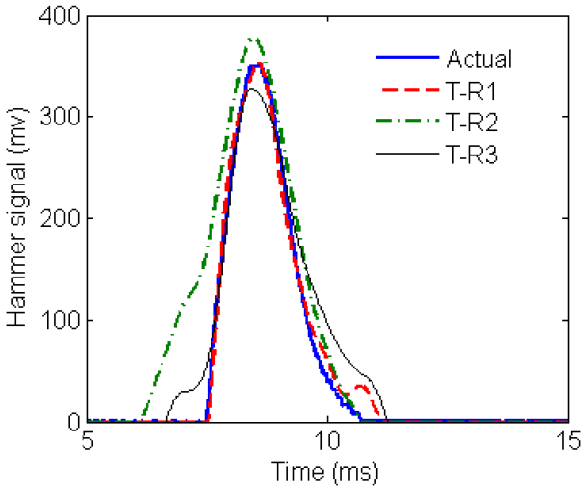

Figure 16. Impact force time-history reconstructions at E_2 (80, −80) by various transfer functions.

were reconstructed successfully. The repeatability of the T-R method for impact loading time-history reconstruction showed the same degree of accuracy compared to that for impact location detection. The good estimation of the peak force and the similar deviation in the main wave packet reconstruction in three impact tests show the robustness of the T-R method for identifying the impact loading time-history.

In impact source identification by the T-R method, both the impact location detection and force reconstruction are based on the transfer functions. However, only a limited number of locations on the plate have been calibrated. The impact locations were often not detected at the calibration locations and the transfer function at the detected impact location should be approximated to reconstruct the impact loading time-history. Figure 16 shows the results of force reconstruction at E_2 (80, −80) by various transfer functions, where T-R1 is by the actual empirical transfer functions at E_2, T-R2 is the approximated transfer functions at the detected impact location (85.6, −78.9) using equation (7), and T-R3 is by the transfer function at calibration point (120, −40), at which the peak value of the reconstructed signals was maximum. The impact loading time-history was reconstructed successfully by three groups of transfer functions. The deviations in the results by two groups of approximated transfer functions were minor though they were not as good as that of actual transfer functions. For the force reconstruction technique, the transfer functions at detected impact locations were approximated by four calibrated transfer functions because their stability was better than that of one calibrated transfer function.

In the impact location detection discussion, the error increases with the increase of the transfer function calibration spacing. In the previous simulation work [14], the error of impact location detection was constrained by the transfer function calibration spacing, and the deviation in force reconstruction increased with the increase of the error in impact location detection. In selection of transfer function spacing, both the error in impact location detection and the deviation in force reconstruction should be considered. Figure 17 shows the impact force time-history reconstructed with various distances from the actual impact location, where the actual impact location is C_1 (−120, −120) and the force was reconstructed at the points from C_1 to B_1 (0, −120) by the transfer functions at these points with spacing 20 mm. The results of four reconstructions when the distances were 20 mm and 60 mm were close to the results of 0 mm and 40 mm respectively. The result of force reconstruction when the distance was 120 mm was worse than that of 100 mm. Table 2 shows the peak force reconstructed under various distances from the actual impact location. As the shapes of the impact forces reconstructed under various distances were different and the transfer functions in small regions were similar to each other, the identified peak force did not decrease with the increase of distance exactly as that of simulation work. It is noteworthy that the impact loading time-history was still reconstructed well when the distance was 80 mm. The error in peak force identification was less than 15.1% if the error in impact location was smaller than 80 mm. In the impact location discussion, the error in impact location detection was less than the spacing of the transfer function calibration locations. Considering both the impact location detection and force reconstruction, the transfer function with a spacing of 80 mm can supply enough information for impact

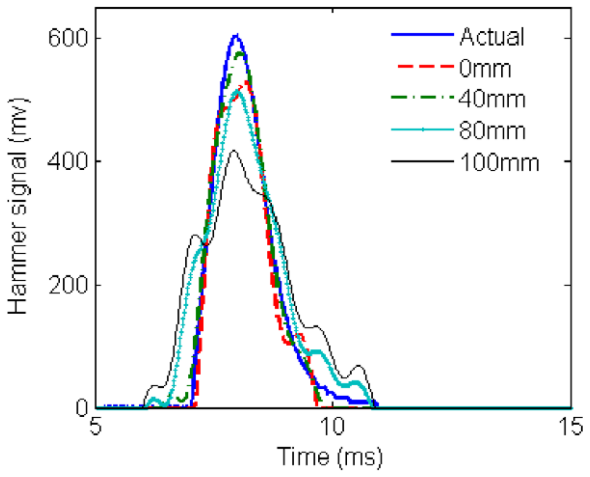

Figure 17. Impact force time-history reconstruction with various distances from the actual impact location.

source identification on a flat aluminum plate with thickness 3.1 mm by the T-R method.

5. Conclusions

The T-R method with associated signal processing algorithms for impact source identification has been verified by a series of impact experiments on a square aluminum plate using a small set of piezoelectric sensors. Both the impact location and the impact loading time-history of the impact force on the entire plate have been estimated successfully. In the validation of the experimental system for the T-R method, the response of the sensors, the linearity of the transfer functions, and the self-focusing capability of the T-R method were analyzed. The method to select the appropriate transfer function spacing was developed. The effect of the calibration location spacing on impact location detection and force reconstruction has been examined in detail. Most impacts were detected at the actual impact area, except a few that were detected at neighboring impact areas when the spacing of the transfer functions was 80, 120, and 160 mm. With increasing calibration location spacing, the success rate of impact area determination decreases, and the average error in impact location detection increases. The average error in impact location detection is about half of the distance between the calibration points when the spacing is 80 mm. Good repeatability of the T-R method for both impact location detection and force reconstruction has been demonstrated empirically.

Approximated transfer functions can be used to reconstruct the impact loading time-history. The deviation in force reconstruction depends on the error in impact location detection and the relative position of the impact location on the plate. The error in peak force identification is less than 15% if the error in impact location is limited by 80 mm. The appropriate spacing of the transfer function was 80 mm for both impact location detection and force reconstruction on this aluminum plate with thickness 3 mm. It is noted that only transfer functions and strain response measured by four sensors are needed for both the impact location detection and the force reconstruction. The T-R technique for the impact source identification is stable and the ill-conditioned inverse problem has been overcome. The T-R method is well suited to monitor impact events on plate-like structures in near real-time. In future work, the T-R method will be further developed to identify the impact source on complex structures including composites and metallic plates with stiffeners.

Acknowledgments

Mr Chen acknowledges support from the National 111 project ‘The center for Mechanical Behavior of Advanced Structures and Materials’ at the Northwestern Polytechnical University. This paper is partially supported by USDOT Grant no RITARS11HUMD through the Commercial Remote Sensing & Spatial Information (CRS&SI) program.

References

[1] Schäer F and Janovsky R 2007 Impact sensor network for detection of hypervelocity impacts on spacecraft *Acta Astronaut.* **61** 901–11
[2] Park J, Hu S and Chang F-K 2009 Monitoring impact events using a system-identification method *AIAA J.* **47** 2011–21
[3] Hu N, Fukunaga H, Matsumoto S, Yan B and Peng X H 2007 *Int. J. Impact Eng.* **34** 1258–71
[4] LeClerc J R, Worden K and Haywood J 2007 Impact detection in an aircraft composite panel—A neural-network approach *J. Sound Vib.* **299** 672–82
[5] Ciampa F and Meo M 2012 Impact detection in anisotropic materials using a time reversal approach *Struct. Health Monit.* **11** 43–9
[6] Qiu L, Yuan S F, Zhang X and Wang Y 2011 A time reversal focusing based impact imaging method and its evaluation on complex composite structures *Smart Mater. Struct.* **20** 105014
[7] Chang C and Sun C T 1989 Determining transverse impact force on a composite laminate by signal deconvolution *Exp. Mech.* **29** 414–9
[8] Jang T S, Hyoungsu B, Han S L and Kinoshita T 2010 Indirect measurement of the impulsive load to a nonlinear system from dynamic responses: inverse problem formulation *Mech. Syst. Signal Process.* **24** 1665–81
[9] Inoue H, Harrigan J J and Reid S R 2001 Review of inverse analysis for indirect measurement of impact force *Appl. Mech. Rev.* **54** 503–24
[10] Seydel R and Chang F K 2001 Impact identification of stiffened composite panels: I. System development *Smart Mater. Struct.* **10** 354–69
[11] Seydel R and Chang F K 2001 Impact identification of stiffened composite panels: II. Implementation studies *Smart Mater. Struct.* **10** 370–9
[12] Chandrashekhara K, Chukwujekwu O A and Jiang Y P 1998 Estimation of contact force on composite plates using impact-induced strain and neural networks *Composites* B **29** 4363–70
[13] Chen C and Yuan F G 2010 Impact source identification in finite isotropic plates using time-reversal method: theoretical study *Smart Mater. Struct.* **19** 105028
[14] Chen C, Li Y and Yuan F G 2011 Development of time-reversal method for impact source identification on plate structures *Shock Vib.* at press